

On an interior-exterior nonoverlapping domain decomposition method for the Poisson–Boltzmann equation

Xuanyu Liu¹, Yvon Maday², Chaoyu Quan³, and Hui Zhang⁴

¹School of Mathematical Sciences, Beijing Normal University, Beijing, China
(xyliu9535@mail.bnu.edu.cn).

²Sorbonne Université, CNRS, Université de Paris, Laboratoire Jacques-Louis Lions (LJLL),
F-75005 Paris, France (maday@ann.jussieu.fr)

³SUSTech International Center for Mathematics, and Department of Mathematics, Southern
University of Science and Technology, Shenzhen, China (quancy@sustech.edu.cn).

⁴Department of Mathematical Sciences, Xi'an Jiaotong-Liverpool University, Suzhou, Jiangsu,
China (hui.zhang@xjtlu.edu.cn).

Abstract

A nonoverlapping domain decomposition method is studied for the linearized Poisson–Boltzmann equation, which is essentially an interior-exterior transmission problem with bounded interior and unbounded exterior. This problem is different from the classical Schwarz alternating method for bounded nonoverlapping subdomains well studied by Lions in 1990, and is challenging due to the existence of unbounded subdomain. To obtain the convergence, a new concept of interior-exterior Sobolev constant is introduced and a spectral equivalence of related Dirichlet-to-Neumann operators is established afterwards. We prove rigorously that the spectral equivalence results in the convergence of interior-exterior iteration. Some numerical simulations are provided to investigate the optimal stepping parameter of iteration and to verify our convergence analysis.

Keywords. domain decomposition, convergence analysis, Poisson–Boltzmann equation

1 Introduction

Many chemical reactions of interest take place in solution where the solvation effect plays an important role and should not be ignored. To characterize the solvation effect, various solvation models have been proposed that can generally be divided into two classes: explicit solvent models and implicit solvent models. The explicit models provide a physical spatially resolved description of the solvent and usually have better simulation comparing to practical experiments, but they are often computationally consuming. The implicit models

characterize the solvent in terms of its macroscopic physical properties, such as the solvent dielectric permittivity and the ionic strength, and are computationally more efficient.

In this article, we are concerned with a representative and widely-used implicit solvation model, the Poisson–Boltzmann (PB) solvation model [1, 2, 3]. In particular, we consider the linearized Poisson–Boltzmann (LPB) equation for simplicity in the form of

$$\begin{cases} -\Delta\psi(\mathbf{x}) = 4\pi\varepsilon_1^{-1}\rho_m(\mathbf{x}) & \text{in } \Omega, \\ -\Delta\psi(\mathbf{x}) + \kappa^2\psi(\mathbf{x}) = 0 & \text{in } \Omega^c := \mathbb{R}^3 \setminus \Omega, \end{cases} \quad (1.1)$$

with the following two jump conditions on the solute-solvent interface $\Gamma := \partial\Omega$,

$$\begin{cases} \psi|_\Omega = \psi|_{\Omega^c} & \text{on } \Gamma, \\ \varepsilon_1\partial_{\mathbf{n}}\psi|_\Omega = \varepsilon_2\partial_{\mathbf{n}}\psi|_{\Omega^c} & \text{on } \Gamma. \end{cases} \quad (1.2)$$

Here, ψ is the unknown electrostatic potential, ρ_m is the solute’s charge distribution supported in the solute cavity Ω , $\kappa > 0$ is the modified Debye–Hückel constant, \mathbf{n} is the unit normal vector pointing outward from Ω to Ω^c , and $0 < \varepsilon_1 \leq \varepsilon_2 < \infty$ are the permittivity constants of the solute and the solvent respectively. In the following content, we make the assumptions that the potential ψ tends to 0 as $|\mathbf{x}|$ tends to infinity and Ω is a bounded Lipschitz domain.

When $\kappa = 0$, the LPB model becomes the polarizable continuum model (PCM) that is also popular in the calculation of solvation energy [4]. When $\kappa = \infty$, i.e., the solvent is treated ideally as perfect conductor, the LPB model becomes a Poisson equation defined only on Ω and is called the conductor-like screening model (COSMO) [5].

Generally speaking, there are three types of widely-used methods to solve the PB model: boundary element method (BEM), finite difference method (FDM) and finite element method (FEM). In the BEM, the LPB equation is recast as integral equations defined on the two-dimensional solute-solvent interface. Then surface meshes are generated (for example, using MSMS [6] or NanoShaper [7]) to solve the integral equations. The BEM is efficient to solve the LPB equation especially when acceleration techniques are used, such as the fast multipole method [8, 9, 10] and the hierarchical “treecode” technique [11, 12]. However, the BEM has a limitation that it is difficult to be applied to the nonlinear Poisson–Boltzmann (NPB) equation. To solve the NPB equation, there have been some efficient FDM solvers including UHBD [13], DelPhi [14], MIBPB [15], and APBS [16, 17, 18]. In particular, the APBS developed by Baker, Holst, McCammon et al. is popular and has many useful options. The FEM provides in general more flexibility for mesh refinement, more analysis of convergence and more selections of linear solvers. A rigorous solution and approximation theory of the FEM for the PB equation has been established in [19]. The adaptive FEM developed by Holst et al. has tackled some important issues of the PB equation [20, 21]. Note that the BEM and FEM are mesh-dependent where the mesh generation itself might be complicated. The FDM depends on grid and the grid refinement in three dimension could result in dramatic increase of computational cost.

A special domain decomposition (dd) method was developed in 2013 by Cancès, Maday, and Stamm for the COSMO model in van der Waals cavity [22], called ddCOSMO, which is meshless and could perform up to three orders of magnitude faster than the equivalent algorithm in Gaussian as shown in [23, 24, 25]. This method highlights that the solute cavity Ω is decomposed into balls and the original problem is changed to be a group of easy-to-solve Laplace subproblems defined in balls. Later, the ddCOSMO solver has been generalized to the PCM and LPB models respectively called ddPCM [26] and ddLPB methods [27], as well as the PCM with smooth interface [28, 29].

On the convergence analysis, ddCOSMO method has linear scaling with respect to the number of atoms and the first results on these scaling properties in a simplified setting can be found in a series of works by Ciaramella and Gander [30, 31, 32]. Recently, Reusken and Stamm propose specific geometrical descriptors and show how the convergence rate of ddCOSMO solver depends on them [33]. Despite plenty of works on the convergence of ddCOSMO, the convergence of ddLPB is still challenging. The difficulty of this convergence lies in the interior-exterior iteration. At each iteration, the ddLPB method first solves the interior Poisson equation and the exterior screening Poisson equation respectively, with the same Dirichlet boundary condition on $\partial\Omega$ obtained from the previous iteration. Then it updates this Dirichlet boundary condition based on the resolved solutions. This procedure is repeated until some stopping criterion is reached.

Note that in the classical works [34, 35], Lions study the Schwarz alternating methods for overlapping and nonoverlapping bounded subdomains respectively, which are nevertheless not our case due to the existence of unbounded exterior subdomain Ω^c . See Figure 1 for a schematic diagram of different types of domain decomposition. The unboundedness of Ω^c makes the convergence analysis challenging.

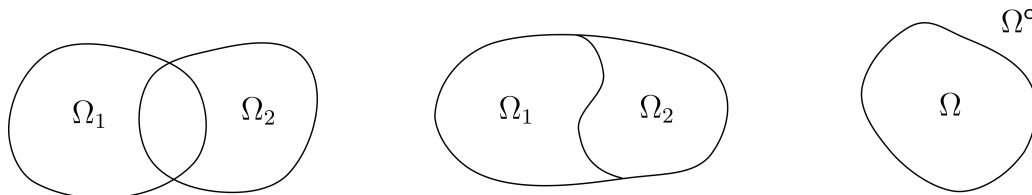


Figure 1: Schematic diagram of different types of domain decomposition, including three cases: overlapping bounded subdomains [34] (left), nonoverlapping bounded subdomains [35] (middle), and nonoverlapping interior-exterior subdomains (right).

In this article, we want to prove the convergence of the interior-exterior iteration for the ddLPB method, which is a nonoverlapping Schwarz alternating method with bounded interior and unbounded exterior. First of all, we generalize the original ddLPB method by adding a stepping parameter for the interfacial iteration on Γ . Then we show rigorously that the convergence of this iteration will be guaranteed as soon as $T_e + T_c$ is spectrally

equivalent to $T_r + T_c$ in the sense that $\exists C_1, C_2 > 0, \forall g \in H^{\frac{1}{2}}(\Gamma)$,

$$C_1 \langle (T_e + T_c)g, g \rangle \leq \langle (T_r + T_c)g, g \rangle \leq C_2 \langle (T_e + T_c)g, g \rangle, \quad (1.3)$$

where T_r, T_c, T_e are Dirichlet-to-Neumann operators defined in (3.3)–(3.5) and $\langle \cdot, \cdot \rangle$ is the duality pairing between $H^{-\frac{1}{2}}(\Gamma)$ and $H^{\frac{1}{2}}(\Gamma)$. This proof is based on constructing a new inner product $\langle \cdot, \cdot \rangle_{ec}$ on the Banach space $H^{\frac{1}{2}}(\Gamma)$. With the help of a newly-defined interior-exterior Sobolev constant C_S , an interior-exterior estimation is obtained

$$\|u_r\|_{L^2(\Omega)}^2 \leq C_S \varepsilon_2^{-1} \kappa^{-2} \langle T_c g, g \rangle \quad \forall g \in H^{\frac{1}{2}}(\Gamma), \quad (1.4)$$

where u_r is a harmonic function with Dirichlet boundary condition g . This estimation results in the desired spectral equivalence above, so that the convergence holds.

The article is organized as follows. In Section 2, we recall and generalize the original ddLPB method by adding a stepping parameter $\alpha \in \mathbb{R}$ for the interfacial iteration. In Section 3, we prove the convergence of the ddLPB method step by step: First, the spectral equivalence can lead to the convergence; second, an interior-exterior estimation allows to establish the spectral equivalence. In Section 4, some numerical simulations are illustrated to verify our analysis. Some concluding remarks are given in the last section.

2 Generalized ddLPB method

We first recall briefly the ddLPB method for the linearized Poisson–Boltzmann equation and then generalize it by adding a stepping parameter for the interior-exterior iterations.

2.1 Interior-interior transmission problem

Given the solute’s charge distribution ρ_m supported in the solute cavity Ω . Let ψ_0 be the potential generated by ρ_m in vacuum satisfying

$$-\Delta \psi_0 = 4\pi \varepsilon_1^{-1} \rho_m \quad \text{in } \mathbb{R}^3. \quad (2.1)$$

In fact, ψ_0 can be obtained explicitly by calculating the following integral:

$$\psi_0(\mathbf{x}) = \int_{\mathbb{R}^3} \frac{\rho_m(\mathbf{y})}{\varepsilon_1 |\mathbf{x} - \mathbf{y}|} d\mathbf{y}, \quad \mathbf{x} \in \mathbb{R}^3. \quad (2.2)$$

For simplicity, we assume that ψ_0 is already given. Then, (1.1) can be recast equivalently to two coupled partial differential equations (PDEs) both defined in Ω (see [27] for the derivation):

$$\begin{cases} -\Delta \psi_r = 0 & \text{in } \Omega, \\ -\Delta \psi_e + \kappa^2 \psi_e = 0 & \text{in } \Omega, \end{cases} \quad (2.3)$$

with two coupling conditions

$$\begin{cases} \psi_r = \psi_e - \psi_0 & \text{in } \Gamma, \\ \psi_e = \mathcal{S}_\kappa (\partial_{\mathbf{n}} \psi_e - \varepsilon_1 \varepsilon_2^{-1} \partial_{\mathbf{n}} (\psi_r + \psi_0)) & \text{in } \Gamma, \end{cases} \quad (2.4)$$

where $\psi_r = \psi|_\Omega - \psi_0$ is the reaction potential and ψ_e is an extended potential, both defined in Ω . Here, $\mathcal{S}_\kappa : H^{-\frac{1}{2}}(\Gamma) \rightarrow H^{\frac{1}{2}}(\Gamma)$ is the invertible single-layer operator

$$(\mathcal{S}_\kappa \sigma)(\mathbf{x}) := \int_\Gamma \frac{\exp(-\kappa |\mathbf{x} - \mathbf{s}'|) \sigma(\mathbf{s}')}{4\pi |\mathbf{x} - \mathbf{s}'|} d\mathbf{s}' \quad \forall \sigma \in H^{-\frac{1}{2}}(\Gamma), \mathbf{x} \in \Gamma. \quad (2.5)$$

Further, we recall the potential $\tilde{\mathcal{S}}_\kappa : H^{-\frac{1}{2}}(\Gamma) \rightarrow H^1(\mathbb{R}^3 \setminus \Gamma)$ associated with the homogeneous screening Poisson (HSP) equation in (2.3), defined by

$$(\tilde{\mathcal{S}}_\kappa \sigma)(\mathbf{x}) := \int_\Gamma \frac{\exp(-\kappa |\mathbf{x} - \mathbf{s}'|) \sigma(\mathbf{s}')}{4\pi |\mathbf{x} - \mathbf{s}'|} d\mathbf{s}' \quad \forall \sigma \in H^{-\frac{1}{2}}(\Gamma), \mathbf{x} \in \mathbb{R}^3 \setminus \Gamma. \quad (2.6)$$

In particular, when $\kappa = 0$, the HSP equation becomes the Laplace equation, and we use the \mathcal{S}_0 and $\tilde{\mathcal{S}}_0$ to denote the corresponding single-layer operator and potential for Laplace equation.

The initial problem (1.1) defined in \mathbb{R}^3 is transformed equivalently into two subproblems (2.3) defined in Ω and coupled on the interface Γ with conditions (2.4). This means that the original interior-exterior transmission problem is actually recasted to an interior-interior transmission problem.

2.2 Generalization

The ddLPB method updates the potential on solute-solvent interface at each external iteration. We now generalize the ddLPB method proposed in [27]. The new procedure still includes five steps as shown in Algorithm 1. Comparing to the original ddLPB method (where $\alpha = 1$ in step 4), we now take a stepping parameter $\alpha \in \mathbb{R}$ that controls the step size.

We will show that the generalized method is convergent if α satisfies one simple restriction. Choosing this parameter could affect the convergence rate significantly. Consequently a suitable choice of α can speed up the algorithm by reducing the number of external iterations.

3 Convergence analysis

It was observed from the numerical experiments in [27] that the interfacial iteration in the ddLPB procedure converges quickly with respect to (w.r.t.) the iteration number k . We prove this convergence theoretically in this section.

Algorithm 1 ddLPB method

1. Let g^0 be an initial guess of $\psi_e|_\Gamma$ and set the iteration number to $k = 1$.
2. Solve the Laplace equation

$$\begin{cases} -\Delta\psi_r^k = 0 & \text{in } \Omega, \\ \psi_r^k = g^{k-1} - \psi_0 & \text{on } \Gamma, \end{cases} \quad (2.7)$$

and obtain its Neumann boundary trace $\partial_{\mathbf{n}}\psi_r^k$ on Γ .

3. Solve the screened Poisson equation

$$\begin{cases} -\Delta\psi_e^k + \kappa^2\psi_e^k = 0 & \text{in } \Omega, \\ \psi_e^k = g^{k-1} & \text{on } \Gamma, \end{cases} \quad (2.8)$$

and obtain its Neumann boundary trace $\partial_{\mathbf{n}}\psi_e^k$ on Γ .

4. Update the Dirichlet boundary condition

$$g^k = (1 - \alpha)g^{k-1} + \alpha \mathcal{S}_\kappa \left[\partial_{\mathbf{n}}\psi_e^k - \varepsilon_1\varepsilon_2^{-1}\partial_{\mathbf{n}}(\psi_0 + \psi_r^k) \right] \quad (2.9)$$

with an appropriate constant $\alpha \in \mathbb{R}$.

5. Compute the electrostatic solvation energy E_k from ψ_r^k at k -th iteration, set $k \leftarrow k+1$, and repeat step 2–5 until $|E_k - E_{k-1}|/|E_{k-1}| < \mathbf{tol}$ for some given tolerance \mathbf{tol} .
-

More precisely, we first show that the interfacial iteration in the ddLPB solver is essentially a modified Richardson iteration. Then, we prove the convergence on the continuous level by establishing the spectral equivalence of some Dirichlet-to-Neumann (DtN) operators, where a suitable subspace of $H^{\frac{1}{2}}(\Gamma)$ is chosen and a new concept of interior-exterior Sobolev constant is proposed. discrete level, which is more challenging than the continuous case.

3.1 Richardson iteration

In the generalized ddLPB solver, the interfacial iteration is essentially a modified Richardson iteration.

In fact, the LPB problem (2.3)–(2.4) can be seen as an interface problem: Find $g \in H^{\frac{1}{2}}(\Gamma)$, satisfying

$$T_r(g - \psi_0) + \varepsilon_1\partial_{\mathbf{n}}\psi_0 + T_c g = 0, \quad (3.1)$$

that is,

$$(T_r + T_c)g = -\varepsilon_1 \partial_{\mathbf{n}} \psi_0 + T_r \psi_0, \quad (3.2)$$

where $T_r : g \mapsto \varepsilon_1 \partial_{\mathbf{n}} u_r$ is a DtN operator in the bounded domain Ω , satisfying

$$\begin{cases} -\Delta u_r = 0 & \text{in } \Omega, \\ u_r = g & \text{on } \Gamma, \end{cases} \quad (3.3)$$

and $T_c : g \mapsto -\varepsilon_2 \partial_{\mathbf{n}} u_c$ is another DtN operator in the exterior domain Ω^c , satisfying

$$\begin{cases} -\Delta u_c + \kappa^2 u_c = 0 & \text{in } \Omega^c, \\ u_c = g & \text{on } \Gamma. \end{cases} \quad (3.4)$$

Remember that \mathbf{n} is the unit normal vector on Γ pointing from Ω to Ω^c . Furthermore, we define the following DtN operator $T_e : g \mapsto \varepsilon_2 \partial_{\mathbf{n}} u_e$, satisfying

$$\begin{cases} -\Delta u_e + \kappa^2 u_e = 0 & \text{in } \Omega, \\ u_e = g & \text{on } \Gamma. \end{cases} \quad (3.5)$$

For any $g \in H^{\frac{1}{2}}(\Gamma)$, the corresponding surface charge density $\sigma \in H^{-\frac{1}{2}}(\Gamma)$ satisfies

$$\begin{cases} g = \mathcal{S}_\kappa \sigma, \\ \sigma = \varepsilon_2^{-1} (T_e + T_c) g, \end{cases} \quad (3.6)$$

which yields that

$$g = \varepsilon_2^{-1} \mathcal{S}_\kappa (T_e + T_c) g \quad \forall g \in H^{\frac{1}{2}}(\Gamma). \quad (3.7)$$

Therefore, we have

$$(T_e + T_c)^{-1} = \varepsilon_2^{-1} \mathcal{S}_\kappa : H^{-\frac{1}{2}}(\Gamma) \rightarrow H^{\frac{1}{2}}(\Gamma), \quad (3.8)$$

that is invertible. We take $\varepsilon_2^{-1} \mathcal{S}_\kappa$ as a preconditioner for (3.2), to obtain

$$\varepsilon_2^{-1} \mathcal{S}_\kappa [-(T_r + T_c)g + (-\varepsilon_1 \partial_{\mathbf{n}} \psi_0 + T_r \psi_0)] = 0. \quad (3.9)$$

This equation can be solved by the modified Richardson iteration as follows:

$$g^{k+1} = g^k + \alpha \varepsilon_2^{-1} \mathcal{S}_\kappa [-(T_r + T_c)g^k + (-\varepsilon_1 \partial_{\mathbf{n}} \psi_0 + T_r \psi_0)], \quad (3.10)$$

where $\alpha \in \mathbb{R}$ is an appropriate scalar parameter. From another point of view, (3.10) can be reformulated as

$$\begin{aligned} g^{k+1} &= (1 - \alpha) g^k + \alpha \varepsilon_2^{-1} \mathcal{S}_\kappa [T_e g^k - T_r (g^k - \psi_0) - \varepsilon_1 \partial_{\mathbf{n}} \psi_0] \\ &= (1 - \alpha) g^k + \alpha \varepsilon_2^{-1} \mathcal{S}_\kappa [\varepsilon_2 \partial_{\mathbf{n}} \psi_e^k - \varepsilon_1 \partial_{\mathbf{n}} \psi_r^k - \varepsilon_1 \partial_{\mathbf{n}} \psi_0] \\ &= (1 - \alpha) g^k + \alpha \mathcal{S}_\kappa [\partial_{\mathbf{n}} \psi_e^k - \varepsilon_1 \varepsilon_2^{-1} \partial_{\mathbf{n}} (\psi_r^k + \psi_0)], \end{aligned} \quad (3.11)$$

that coincides with the iteration formula (2.9) used in the generalized ddLPB solver.

3.2 Relationship between convergence and spectral equivalence

We first recall some preliminary results on the spectrum of linear operator in the following lemma.

Proposition 3.1 (Properties on spectrum, [36]). *Let X, Y be two Banach spaces and $L(X, Y)$ be the spaces for bounded linear operators from X to Y . There are some facts as follows:*

1. *If $A \in L(X, X)$ and $P(x)$ is a polynomial, then we have*

$$\rho(P(A)) = \{P(\lambda) : \lambda \in \sigma(A)\}, \quad (3.12)$$

where $\rho(A)$ is the spectrum of the operator A .

2. *If $A \in L(X, X)$, then $\lim_{n \rightarrow \infty} \|A^n\|_{L(X, X)}^{\frac{1}{n}} = \rho(A)$ where $\rho(A) := \sup_{\lambda \in \rho(A)} |\lambda|$ is the spectral radius of A .*
3. *(Spectral inclusion) If H is a Hilbert space with the inner product $\langle \cdot, \cdot \rangle_H$ and $T \in L(H, H)$, then*

$$\rho(T) \subset \overline{W(T)} \quad \text{where} \quad W(T) := \{\langle Tg, g \rangle_H : g \in H, \langle g, g \rangle_H = 1\}. \quad (3.13)$$

Proof. See [36, Lemma 1 following Theorem VII.1, Theorem VI.6] and [37, Theorem 1.2-1]. \square

The following theorem shows that the convergence of iteration (3.10) can be deduced from the spectral equivalence of $T_e + T_c$ and $T_r + T_c$.

Theorem 3.1. *Suppose that $T_e + T_c$ is spectrally equivalent to $T_r + T_c$, in the sense that $\exists 0 < C_1 \leq C_2$,*

$$C_1 \langle (T_e + T_c)g, g \rangle \leq \langle (T_r + T_c)g, g \rangle \leq C_2 \langle (T_e + T_c)g, g \rangle \quad \forall g \in H^{\frac{1}{2}}(\Gamma), \quad (3.14)$$

where $\langle \cdot, \cdot \rangle$ is the duality pairing between $H^{-\frac{1}{2}}(\Gamma)$ and $H^{\frac{1}{2}}(\Gamma)$. Then the spectrum of $(T_e + T_c)^{-1}(T_r + T_c)$ is bounded as follows

$$\rho((T_e + T_c)^{-1}(T_r + T_c)) \subset [C_1, C_2], \quad (3.15)$$

and consequently the iteration (3.10) converges for $0 < \alpha < 2/C_2$.

Proof. We first show the symmetric positive definiteness of the bilinear forms $\langle T_e \cdot, \cdot \rangle$ and $\langle T_c \cdot, \cdot \rangle$. For $g_1, g_2 \in H^{\frac{1}{2}}(\Gamma)$, denote $u_{e,1}$ and $u_{e,2}$ the solutions of (3.5) with the boundary

g_1 and g_2 , respectively. Multiplying $u_{e,2}$ and $u_{e,1}$ on both sides of (3.5) and integrating over Ω , we have

$$\langle T_e g_1, g_2 \rangle = \varepsilon_2 \int_{\Omega} (\nabla u_{e,1} \cdot \nabla u_{e,2} + \kappa^2 u_{e,1} u_{e,2}) = \langle g_1, T_e g_2 \rangle. \quad (3.16)$$

When $g_1 = g_2$, we have

$$\langle T_e g_1, g_1 \rangle = \varepsilon_2 \int_{\Omega} (|\nabla u_{e,1}|^2 + \kappa^2 u_{e,1}^2) \geq 0. \quad (3.17)$$

When $\langle T_e g_1, g_1 \rangle = 0$, the fact that $\kappa > 0$ yields $u_{e,1} = 0$, which implies $g_1 = u_{e,1}|_{\Gamma} = 0$. Thus, $\langle T_e \cdot, \cdot \rangle$ is symmetric positive-definite on $H^{\frac{1}{2}}(\Gamma)$. A similar argument shows that $\langle T_c \cdot, \cdot \rangle$ is also symmetric positive-definite on $H^{\frac{1}{2}}(\Gamma)$.

Since $\langle T_e \cdot, \cdot \rangle$ and $\langle T_c \cdot, \cdot \rangle$ are symmetric positive-definite, we can define a new inner product on $H^{\frac{1}{2}}(\Gamma)$ as follows

$$\langle g_1, g_2 \rangle_{ec} := \langle (T_e + T_c)g_1, g_2 \rangle \quad \forall g_1, g_2 \in H^{\frac{1}{2}}(\Gamma). \quad (3.18)$$

Denote the induced norm in $(H^{\frac{1}{2}}(\Gamma), \langle \cdot, \cdot \rangle_{ec})$ by

$$\|g\|_{ec} := \sqrt{\langle g, g \rangle_{ec}}. \quad (3.19)$$

Then we show $(H^{\frac{1}{2}}(\Gamma), \langle \cdot, \cdot \rangle_{ec})$ is a Hilbert space. For any $g \in H^{\frac{1}{2}}(\Gamma)$, denote u_e and u_c the solutions of (3.5) and (3.4), respectively. A similar argument as (3.17) gives

$$\|g\|_{ec}^2 = \varepsilon_2 \int_{\Omega} (|\nabla u_e|^2 + \kappa^2 u_e^2) + \varepsilon_2 \int_{\Omega^c} (|\nabla u_c|^2 + \kappa^2 u_c^2) \geq C \|u_e\|_{H^1(\Omega)}^2, \quad (3.20)$$

where C depends on ε_2 and κ . This together with the fact that the trace operator $\gamma_0 : H^1(\Omega) \rightarrow H^{\frac{1}{2}}(\Gamma)$ is bounded [38, Theorem 2.6.8], gives

$$\|g\|_{H^{\frac{1}{2}}(\Gamma)}^2 \leq C \|u_e\|_{H^1(\Omega)}^2 \leq C \|g\|_{ec}^2. \quad (3.21)$$

According to [38, Theorem 2.7.7, Theorem 2.10.4, Theorem 2.10.7], we have

$$\|(T_e + T_c)g\|_{H^{-\frac{1}{2}}(\Gamma)} \leq C (\|u_e\|_{H^1(\Omega)} + \|u_c\|_{H^1(\Omega^c)}) \leq C \|g\|_{H^{\frac{1}{2}}(\Gamma)}, \quad (3.22)$$

implying

$$\|g\|_{ec}^2 = \langle (T_e + T_c)g, g \rangle \leq \|(T_e + T_c)g\|_{H^{-\frac{1}{2}}(\Gamma)} \|g\|_{H^{\frac{1}{2}}(\Gamma)} \leq C \|g\|_{H^{\frac{1}{2}}(\Gamma)}^2. \quad (3.23)$$

Combining (3.21) and (3.23), we conclude that the norm $\|\cdot\|_{ec}$ is equivalent to $\|\cdot\|_{H^{\frac{1}{2}}(\Gamma)}$. The Cauchy sequence in $H^{\frac{1}{2}}(\Gamma)$ is also a Cauchy sequence in $(H^{\frac{1}{2}}(\Gamma), \langle \cdot, \cdot \rangle_{ec})$. Since $H^{\frac{1}{2}}(\Gamma)$ is a Banach space, we see that $(H^{\frac{1}{2}}(\Gamma), \langle \cdot, \cdot \rangle_{ec})$ is a Hilbert space.

Now we consider $(T_e + T_c)^{-1}(T_r + T_c) : (H^{\frac{1}{2}}(\Gamma), \langle \cdot, \cdot \rangle_{ec}) \rightarrow (H^{\frac{1}{2}}(\Gamma), \langle \cdot, \cdot \rangle_{ec})$. Since $(T_e + T_c)^{-1} = \varepsilon_2^{-1} \mathcal{S}_\kappa : H^{-\frac{1}{2}}(\Gamma) \rightarrow H^{\frac{1}{2}}(\Gamma)$ is bounded [38, Theorem 3.1.16], combining with the boundedness of T_r and T_c , we know that $(T_e + T_c)^{-1}(T_r + T_c)$ is a bounded operator on $H^{\frac{1}{2}}(\Gamma)$. The equivalence of $\|\cdot\|_{ec}$ and $\|\cdot\|_{H^{\frac{1}{2}}(\Gamma)}$ yields that it is also bounded on $(H^{\frac{1}{2}}(\Gamma), \langle \cdot, \cdot \rangle_{ec})$.

The spectral equivalence condition says that there exist two positive constants C_1, C_2 such that

$$C_1 \langle (T_e + T_c)g, g \rangle \leq \langle (T_r + T_c)g, g \rangle \leq C_2 \langle (T_e + T_c)g, g \rangle \quad \text{for } g \in H^{\frac{1}{2}}(\Gamma). \quad (3.24)$$

Since $\langle (T_e + T_c)^{-1}(T_r + T_c)g, g \rangle_{ec} = \langle (T_r + T_c)g, g \rangle$ and $\|g\|_{ec}^2 = \langle (T_e + T_c)g, g \rangle$, we know from (3.24) and (3.13) that

$$\rho((T_e + T_c)^{-1}(T_r + T_c)) \subset \overline{W((T_e + T_c)^{-1}(T_r + T_c))} \subset [C_1, C_2]. \quad (3.25)$$

Using the first statement of Proposition 3.1 yields

$$\rho(I - \alpha \varepsilon_2^{-1} \mathcal{S}_\kappa (T_r + T_c)) \leq \min \{|1 - \alpha C_2|, |1 - \alpha C_1|\}. \quad (3.26)$$

Then the convergence of the iteration (3.10) can be ensured if

$$\min\{|1 - \alpha C_2|, |1 - \alpha C_1|\} < 1, \quad (3.27)$$

i.e., $0 < \alpha < 2/C_2$. □

According to Theorem 3.1, the convergence of (3.10) will be guaranteed as soon as the spectral equivalence of $T_e + T_c$ and $T_r + T_c$ is proved. Before starting this proof, we propose a new concept of interior-exterior Sobolev constant.

3.3 An interior-exterior Sobolev constant

Given a bounded domain $U \in \mathbb{R}^n$ with C^1 boundary, if $u \in W^{k,p}(U)$ and

$$\frac{1}{q} = \frac{1}{p} - \frac{k}{n} > 0, \quad (3.28)$$

then

$$\|u\|_{L^q(U)} \leq C \|u\|_{W^{k,p}(U)} \quad (3.29)$$

for some Sobolev constant C depending only on k, p, n and U . To establish the spectral equivalence of $T_e + T_c$ and $T_r + T_c$, we now introduce a constant similar to the Sobolev constant, called interior-exterior Sobolev constant, for a given bounded Lipschitz domain U .

Definition 3.1 (interior-exterior Sobolev constant). *Given a bounded Lipschitz domain U with boundary ∂U , the interior-exterior Sobolev constant is defined by*

$$C_S := \sup_{g \neq 0 \in H^{\frac{1}{2}}(\partial U)} \frac{\|u_{\text{in}}\|_{L^2(U)}^2}{\|u_{\text{ex}}\|_{H^1(U^c)}^2}, \quad (3.30)$$

where u_{in} and u_{ex} are respectively the unique solutions to

$$\begin{cases} -\Delta u_{\text{in}} = 0 & \text{in } U, \\ u_{\text{in}} = g & \text{on } \partial U, \end{cases} \quad (3.31)$$

and

$$\begin{cases} -\Delta u_{\text{ex}} + u_{\text{ex}} = 0 & \text{in } U^c, \\ u_{\text{ex}} = g & \text{on } \partial U, \\ u_{\text{ex}} \rightarrow O(|\mathbf{x}|^{-1}) & \text{as } |\mathbf{x}| \rightarrow \infty. \end{cases} \quad (3.32)$$

Note that the existence and uniqueness of u_{in} in (3.31) and u_{ex} in (3.32) are easy to be obtained from Lax-Milgram lemma [38, Theorem 2.10.4, Theorem 2.10.7]. We now claim that C_S is well-defined.

Lemma 3.1. *C_S in (3.30) is well-defined in the sense that $0 < C_S < \infty$.*

Proof. We prove $0 < C_S < \infty$ by contradiction. Assume that there exist a sequence $\{g_n\}_{n=1}^{\infty}$ in $H^{\frac{1}{2}}(\partial U)$ such that

$$\|u_{\text{in},n}\|_{L^2(U)}^2 > n \|u_{\text{ex},n}\|_{H^1(U^c)}^2, \quad (3.33)$$

where $u_{\text{in},n}, u_{\text{ex},n}$ are the solutions to (3.31) and (3.32) with g replaced by g_n .

Without loss of generalization, we assume that $\|u_{\text{in},n}\|_{L^2(U)} = 1$. As a consequence, we have

$$\|u_{\text{ex},n}\|_{H^1(U^c)} \rightarrow 0, \quad (3.34)$$

which means that $u_{\text{ex},n} \rightarrow 0$ and $\nabla u_{\text{ex},n} \rightarrow \mathbf{0}$ weakly. Then, we have

$$g_n = u_{\text{ex},n}|_{\partial U} \rightarrow 0 \quad \text{and} \quad u_{\text{in},n} \rightarrow 0, \quad (3.35)$$

which conflicts with the assumption $\|u_{\text{in},n}\|_{L^2(U)} = 1$. □

With the definition of interior-exterior Sobolev constant, we have the following estimation of the solution to the Laplace equation (3.3).

Lemma 3.2 (interior-exterior estimation). *Given any $g \in H^{\frac{1}{2}}(\Gamma)$, suppose that u_r is the solution to (3.3). Then we have*

$$\|u_r\|_{L^2(\Omega)}^2 \leq C_S \varepsilon_2^{-1} \kappa^{-2} \langle T_c g, g \rangle, \quad (3.36)$$

where C_S is the interior-exterior Sobolev constant defined in (3.30) depending only on Ω .

Proof. For $g \in H^{\frac{1}{2}}(\Gamma)$, we denote by $u_{c,\kappa}$ the solution to (3.4) and by $u_{c,1}$ the solution to (3.32). Multiplying (3.4) with $u_{c,\kappa}$ and integrating over Ω^c , we can obtain

$$\langle T_c g, g \rangle = \varepsilon_2 \int_{\Omega^c} (|\nabla u_{c,\kappa}|^2 + \kappa^2 u_{c,\kappa}^2) \geq 0. \quad (3.37)$$

Further, multiplying $u_{c,\kappa}$ on both sides of (3.32) and integrating over Ω^c , we have

$$\begin{aligned} \|u_{c,1}\|_{H^1(\Omega^c)}^2 &= \int_{\Gamma} (\partial_{\mathbf{n}} u_{c,1}) u_{c,1} = \int_{\Gamma} (\partial_{\mathbf{n}} u_{c,1}) u_{c,\kappa} \\ &= \int_{\Omega^c} (\nabla u_{c,1} \cdot \nabla u_{c,\kappa} + u_{c,1} u_{c,\kappa}) \\ &\leq \frac{1}{2} \int_{\Omega^c} (|\nabla u_{c,\kappa}|^2 + u_{c,\kappa}^2 + |\nabla u_{c,1}|^2 + u_{c,1}^2), \end{aligned} \quad (3.38)$$

which implies that

$$\|u_{c,1}\|_{H^1(\Omega^c)}^2 \leq \int_{\Omega^c} |\nabla u_{c,\kappa}|^2 + u_{c,\kappa}^2. \quad (3.39)$$

Combining this inequality with (3.37), we estimate

$$\|u_{c,1}\|_{H^1(\Omega^c)}^2 \leq \int_{\Omega^c} |\nabla u_{c,\kappa}|^2 + u_{c,\kappa}^2 \leq \varepsilon_2^{-1} \kappa^{-2} \langle T_c g, g \rangle. \quad (3.40)$$

According to the Definition (3.30), we then obtain the stated result. \square

Remark 3.1. *In practical simulations for implicit solvent models, $\kappa > 0$ is usually small.*

The interior-exterior Sobolev constant C_S is important in our convergence analysis. However, the estimation of C_S is as tough as the standard Sobolev constant. In the special case of ball, the standard Sobolev constant can be estimated. But for a general domain, this is a challenging task. In Appendix A, we show the estimation $C_S \leq \frac{1}{3}R^3$ when Ω is an isolated ball with radius R .

3.4 Spectral equivalence

We now prove rigorously the convergence of the ddLPB solver, i.e., the interfacial iteration (3.10). Based on the discussions in subsection 3.2, we realize that the convergence actually results from the spectral equivalence between $T_e + T_c$ and $T_r + T_c$. With the newly-defined interior-exterior Sobolev constant C_S in subsection 3.3, we are ready to state and prove the desired spectral equivalence.

Theorem 3.2 (Spectral equivalence). *There exist two positive constants C_1 and C_2 independent of g , such that $\forall g \in H^{\frac{1}{2}}(\Gamma)$,*

$$C_1 \langle (T_e + T_c) g, g \rangle \leq \langle (T_r + T_c) g, g \rangle \leq C_2 \langle (T_e + T_c) g, g \rangle, \quad (3.41)$$

where

$$C_1 = \min \left\{ \frac{\varepsilon_1}{\varepsilon_2}, \frac{1}{1 + C_S} \right\}, \quad C_2 = \max\{1, \varepsilon_1/\varepsilon_2\}. \quad (3.42)$$

Proof. Multiplying (3.5) by u_e and integrating over Ω , we obtain

$$\langle T_e g, g \rangle = \varepsilon_2 \int_{\Gamma} (\partial_{\mathbf{n}} u_e) u_e = \varepsilon_2 \int_{\Omega} (|\nabla u_e|^2 + \kappa^2 u_e^2). \quad (3.43)$$

Similarly, multiplying (3.3) by u_r and integrating over Ω , we have

$$\langle T_r g, g \rangle = \varepsilon_1 \int_{\Omega} |\nabla u_r|^2. \quad (3.44)$$

Furthermore, multiplying (3.5) by u_r and integrating over Ω , we obtain

$$\langle T_e g, g \rangle = \varepsilon_2 \int_{\Gamma} (\partial_{\mathbf{n}} u_e) u_r = \varepsilon_2 \int_{\Omega} (\nabla u_e \cdot \nabla u_r + \kappa^2 u_e u_r). \quad (3.45)$$

Similarly, multiplying (3.3) by u_e and integrating over Ω , we have

$$\langle T_r g, g \rangle = \varepsilon_1 \int_{\Omega} \nabla u_r \cdot \nabla u_e. \quad (3.46)$$

We now prove the second inequality of (3.41). According to (3.46), we have

$$\langle T_r g, g \rangle \leq \frac{1}{2} \varepsilon_1 \int_{\Omega} (|\nabla u_r|^2 + |\nabla u_e|^2). \quad (3.47)$$

Combined with (3.44) and (3.43), we obtain

$$\frac{1}{2} \langle T_r g, g \rangle \leq \frac{1}{2} \varepsilon_1 \int_{\Omega} |\nabla u_e|^2 \leq \frac{\varepsilon_1}{2\varepsilon_2} \langle T_e g, g \rangle, \quad (3.48)$$

that is,

$$\langle (T_r + T_c)g, g \rangle \leq \max \left\{ \frac{\varepsilon_1}{\varepsilon_2}, 1 \right\} \langle (T_e + T_c)g, g \rangle, \quad (3.49)$$

The remaining question is to prove that there exists a constant $C_2 > 0$ independent g , such that,

$$\langle T_e g, g \rangle \leq C_2 \langle (T_r + T_c)g, g \rangle. \quad (3.50)$$

According to (3.45), we have

$$\langle T_e g, g \rangle \leq \frac{1}{2} \varepsilon_2 \int_{\Omega} (|\nabla u_e|^2 + \kappa^2 u_e^2) + \frac{1}{2} \varepsilon_2 \int_{\Omega} (|\nabla u_r|^2 + \kappa^2 u_r^2), \quad (3.51)$$

that is,

$$\frac{1}{2} \langle T_e g, g \rangle \leq \frac{\varepsilon_2}{2\varepsilon_1} \langle T_r g, g \rangle + \frac{1}{2} \varepsilon_2 \kappa^2 \int_{\Omega} u_r^2, \quad (3.52)$$

obtained from (3.43) and (3.44). Using Lemma 3.2, we then obtain

$$\langle T_e g, g \rangle \leq \frac{\varepsilon_2}{\varepsilon_1} \langle T_r g, g \rangle + C_S \langle T_c g, g \rangle. \quad (3.53)$$

This leads to

$$\langle (T_e + T_c)g, g \rangle \leq \max \left\{ \frac{\varepsilon_2}{\varepsilon_1}, 1 + C_S \right\} \langle (T_r + T_c)g, g \rangle. \quad (3.54)$$

□

Remark 3.2. *One interesting thing is that the spectral equivalence constants C_1 and C_2 do not depend on κ . This means that as $\kappa \rightarrow 0$, i.e., the LPB model becomes polarizable continuum model, the convergence can still be ensured.*

Remark 3.3. *Theorem 3.1 claims that if $0 < \alpha < 2/C_2$ where C_2 is given by (3.42), then (3.10) is convergent. The convergent rate is determined by $\rho(I - \alpha \varepsilon_2^{-1} \mathcal{S}_{\kappa}(T_r + T_c))$, thus by the essential upper bound and lower bound of the spectrum of $\varepsilon_2^{-1} \mathcal{S}_{\kappa}(T_r + T_c)$ and α . If C_1 and C_2 defined in (3.42) is close to the essential lower bound and upper bound of the spectrum of $(T_e + T_c)^{-1}(T_r + T_c)$, then we can choose a better α to speed up the convergence. Specifically, when*

$$\alpha = \alpha_{\text{op}} := \frac{2}{C_1 + C_2}, \quad (3.55)$$

the spectral radius of iteration (3.10) satisfies

$$\rho\left(I - \alpha (T_e + T_c)^{-1} (T_r + T_c)\right) \leq \frac{C_2 - C_1}{C_1 + C_2} < 1. \quad (3.56)$$

For practical solvent models, we have $\varepsilon_1 = 1$ and $\varepsilon_2 > \varepsilon_1$. According to the definition of C_1 and C_2 in (3.42), we then have $C_2 = 1$ and

$$\alpha_{\text{op}} = 2 - \frac{2}{\max\{\varepsilon_2, C_S + 1\} + 1}. \quad (3.57)$$

4 Numerical results

In this section, we do some numerical experiments to verify our convergence analysis for the ddLPB method.

For simplicity, we consider the van der Waals cavity as Ω that can be decomposed into a group of overlapping balls

$$\Omega = \bigcup_{j=1}^M \Omega_j, \quad (4.1)$$

where M is the number of atoms and $\Omega_j \in \mathbb{R}^3$ is the j th atomic ball. We use the ddLPB solver in [27] that solves the internal Laplace and HSP equations in Step 2 and 3 in Algorithm 1 using the idea of overlapping domain “spherical” decomposition. To be precise, for the Laplace equation of ψ_r and the HSP equation of ψ_e , we solve a group of coupled Laplace sub-equations and coupled HSP sub-equations each defined in a ball. Since the Laplace or HSP subproblem in a ball has explicit solution formula, the Laplace and HSP solver in Ω is efficient and has linear scaling. One can refer to [27] for details on the interior solver.

The solutions of (2.7) and (2.8) on each sphere is approximated by a linear combination of spherical harmonics $\{Y_\ell^m\}$ with $0 \leq \ell \leq \ell_{\max}$ and $-\ell \leq m \leq \ell$. At each external iteration, the following linear system needs to be solved

$$\begin{cases} AX_r = G_X + G_0, \\ BX_e = G_X, \end{cases} \quad (4.2)$$

where X_r , X_e and G_X are the vectors of the coefficients of spherical harmonics for ψ_r , ψ_e and g , respectively. In the generalized ddLPB method, we shall update the Dirichlet boundary condition (2.9) numerically as

$$G_X^{(k)} = (1 - \alpha)G_X^{(k-1)} + \alpha(F_0 - C_1X_r^{(k)} - C_2X_e^{(k)}), \quad (4.3)$$

which is slightly different from the original ddLPB method in [27].

By default, we take the dielectric permittivity in the solute cavity as in vacuum, that is to say, $\varepsilon_1 = 1$. Moreover, we set the Debye-Hückel screen constant to $\kappa = 0.1040 \text{ \AA}^{-1}$ for an ionic strength $I = 0.1$ molar. The atomic centers, charges, and VDW radii are obtained from the PDB files [39] and the PDB2PQR [40, 17] package with the setting of PEOEPB force field. The stopping criterion is that the relative error of energy satisfies

$$\mathbf{Err}_k := \frac{|E^{(k)} - E^{(k-1)}|}{|E^{(k-1)}|} < \mathbf{tol} = 10^{-4} \quad (4.4)$$

or the iteration number k reaches $k_{\max} = 60$. In the following tests, we say that the iteration is “convergent” if the iteration stops within 60 steps, i.e., the maximum iteration number k_{\max} is not reached.

4.1 Tests on small molecules

We first test the benzene and caffeine molecules. To run the ddLPB solver, we set the degree of spherical harmonics $\ell_{\max} = 7$ and the number of Lebedev points $N_{\text{leb}} = 86$ (see [27] for details on settings).

4.1.1 Range of stepping parameter for convergence

In Figure 2, we plot the iteration number w.r.t. different choices of $\alpha \in \{0.1, 0.2, \dots, 2.0\}$, respectively for $\varepsilon_2 = 2, 1, 0.5$. Note that here we only draw the point for the iteration number smaller than k_{\max} , i.e., the “convergent” cases.

Theorem 3.1 states that the ddLPB iteration (3.10) shall converge for $0 < \alpha < 2/C_2$ with $C_2 = \max\{1, \varepsilon_1/\varepsilon_2\}$. Therefore, when $\varepsilon_2 = 1$ or 2 , ddLPB will converge for $0 < \alpha < 2$, while when $\varepsilon_2 = 0.5$, ddLPB will converge for $0 < \alpha < 1$. This is indeed observed in Figure 2.

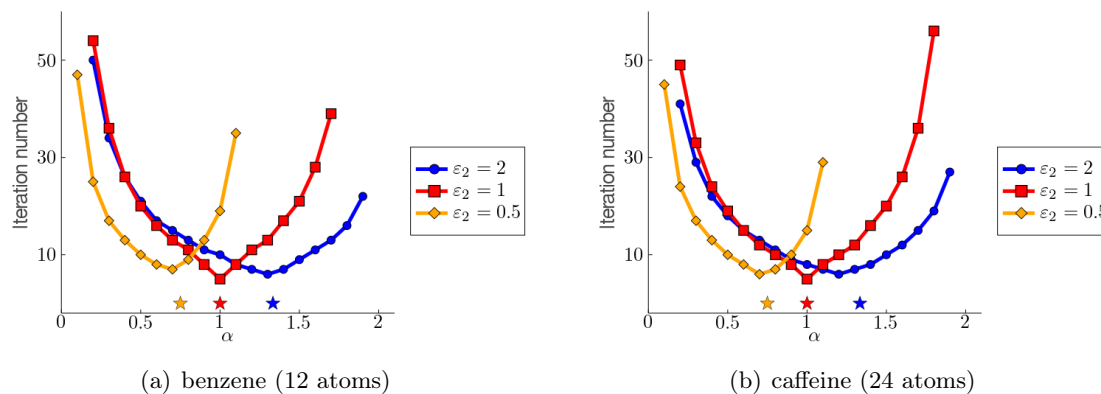


Figure 2: Iteration number $N_{\text{ite}}(\alpha)$ vs the stepping parameter α for small molecules ($\varepsilon_1 = 1$, $\kappa = 0.104\text{\AA}^{-1}$). The optimal parameter α_{op} in (4.7) is the abscissa of star with different colors corresponding different ε_2 .

4.1.2 Theoretical and numerical optimal stepping parameters

When the iteration number reaches the minimum, the corresponding α is denoted by $\tilde{\alpha}_{\text{op}}$, i.e.,

$$\tilde{\alpha}_{\text{op}} = \underset{\alpha \in \{0.1, 0.2, \dots, 2.0\}}{\text{argmin}} N_{\text{ite}}(\alpha), \quad (4.5)$$

where $N_{\text{ite}}(\alpha)$ is the iteration number for a fixed α . According to (3.55), we have

$$\alpha_{\text{op}} = \frac{2}{\min\{\varepsilon_1/\varepsilon_2, 1/(1+C_S)\} + \max\{1, \varepsilon_1/\varepsilon_2\}}. \quad (4.6)$$

Since C_S is difficult to estimate, we simply *ignore the item* $1/(1+C_S)$ in the above equation. As a consequence, we have

$$\alpha_{\text{op}} = \frac{2}{\varepsilon_1/\varepsilon_2 + \max\{1, \varepsilon_1/\varepsilon_2\}} = \frac{4}{3}, 1, \frac{3}{4} \quad \text{for } \varepsilon_2 = 2, 1, 0.5, \text{ respectively.} \quad (4.7)$$

From Figure 2, we observe that for benzene molecule,

$$\tilde{\alpha}_{\text{op}} = 1.3, 1, 0.7 \quad \text{for } \varepsilon_2 = 2, 1, 0.5, \text{ respectively,} \quad (4.8)$$

and for benzene molecule,

$$\tilde{\alpha}_{\text{op}} = 1.3, 1, 0.7 \quad \text{for } \varepsilon_2 = 2, 1, 0.5, \text{ respectively,} \quad (4.9)$$

One can find that α_{op} almost coincides with $\tilde{\alpha}_{\text{op}}$ for different ε_2 , which verify our analysis. On the other hand, this also indicates that in practical implementations of ddLPB algorithm, one might choose α_{op} defined in (4.7) as the guess of optimal stepping parameter, in particular for not large ε_2 .

4.1.3 $\tilde{\alpha}_{\text{op}}$ w.r.t. ε_2

We now test the relationship between $\tilde{\alpha}_{\text{op}}$ and $\varepsilon_2 \geq 1$. The results are shown in Figure 3. In fact, in the case of $\varepsilon_2 \geq 1$, (4.7) becomes

$$\alpha_{\text{op}} = \frac{2}{\varepsilon_2^{-1} + 1}, \quad (4.10)$$

which is plotted as reference curve in Figure 3 (the estimation of C_S has been ignored).

We see that $\tilde{\alpha}_{\text{op}}$ increases as ε_2 increases at the beginning, then when ε_2 is sufficiently large, $\tilde{\alpha}_{\text{op}}$ does not change much. The profile of $\tilde{\alpha}_{\text{op}}$ is quite similar to α_{op} in (4.10), except that $\tilde{\alpha}_{\text{op}}$ is smaller. The reason might be that C_1 is only a lower bound in (3.41), not necessarily the essential infimum. Since the essential infimum could be larger than C_1 , the numerical optimal stepping parameter $\tilde{\alpha}_{\text{op}}$ might be smaller than α_{op} .

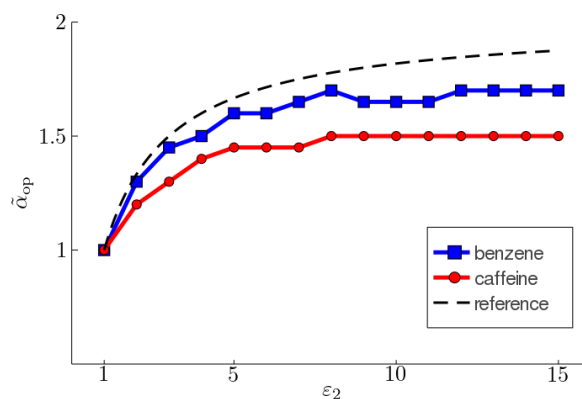


Figure 3: $\tilde{\alpha}_{\text{op}}$ vs ε_2 for benzene and caffeine ($\varepsilon_1 = 1$, $\kappa = 0.104\text{\AA}^{-1}$), and α_{op} in (4.10) is the black dash line.

4.1.4 Water solvent case

We now test the water solvent models for benzene and caffeine. In this case, the dielectric permittivity of water $\varepsilon_2 = 78.54$ at the room temperature $T = 298.15\text{K}$ (25°C). The results of $N_{\text{ite}}(\alpha)$ for $\alpha = 0.1, 0.2, \dots, 2.0$ are presented in Table 1. We observe that iteration is convergent for $\alpha \in (0, 2)$ for these molecules, which agrees with our theory. From this table, $\tilde{\alpha}_{\text{op}}$ is around 1.8 and 1.5 respectively for benzene and caffeine.

Moreover, with different stepping parameters, the computed energies are very close to each other. For the benzene, all computed energies lie in the range $(-0.2068, -0.2063)$, while for caffeine, the range is $(-2.1989, -2.1952)$. This means that with different choices of α , the convergent energies are almost the same, but not the number of iterations. A good choice of α can speed up the algorithm significantly.

Molecules	Number of iterations with different α										Energy range (kJ/mol)
	0.1	0.2	0.3	0.4	0.5	0.6	0.7	0.8	0.9	1.0	
benzene (12)	47	32	24	20	17	15	13	12	11	10	$(-0.2068, -0.2063)$
caffeine (24)	30	22	17	14	12	11	10	9	8	7	$(-2.1989, -2.1955)$
Molecules	Number of iterations with different α										Energy range (kJ/mol)
	1.1	1.2	1.3	1.4	1.5	1.6	1.7	1.8	1.9	2.0	
benzene (12)	9	9	8	7	7	7	6	5	5	7	$(-0.2063, -0.2063)$
caffeine (24)	7	7	6	6	3	5	6	7	8	10	$(-2.1964, -2.1952)$

Table 1: Small molecules in water ($\varepsilon_1 = 1$, $\varepsilon_2 = 78.54$, $\kappa = 0.104 \text{ \AA}^{-1}$).

4.2 Tests on protein molecules

We then test some protein molecules with the PDB codes 1a3y, 2olx, 1yjo, 1etn, ala25 and 1bbl. To run the ddLPB solver, we set $\ell_{\text{max}} = 7$ and $N_{\text{lev}} = 86$ for 1a3y, 2olx, 1yjo, 1etn and ala25. But for 1bbl with 576 atoms, we set $\ell_{\text{max}} = 5$ and $N_{\text{lev}} = 50$ due to the huge computational cost in Matlab.

With the same settings as Figure 2, we plot in Figure 4 the iteration number w.r.t. different choices of $\alpha \in \{0.1, 0.2, \dots, 2.0\}$, respectively for $\varepsilon_2 = 2, 1, 0.5$. We still observe

that when $\varepsilon_2 = 1, 2$, the ddLPB is convergent for $\alpha \in (0, 2)$, while when $\varepsilon_2 = 0.5$, the ddLPB converges for $\alpha \in (0, 1)$, which perfectly matches Theorem 3.1. Moreover, we still see from Figure 4 that α_{op} in (4.7) is close to $\bar{\alpha}_{\text{op}}$.

We now test the water solvent models with $\varepsilon_2 = 78.54$ for the above protein molecules. The results of $N_{\text{ite}}(\alpha)$ for $\alpha = 0.1, 0.2, \dots, 2.0$ are presented in Table 2. For a given protein molecule, the computed energies with different α are close to each other, despite of the number of iterations. It seems that $\alpha = 1.7$ is always a good choice for acceleration. Compared to the original ddLPB ($\alpha = 1$), taking $\alpha = 1.7$ in the generalized ddLPB can reduce the number of iterations and consequently save the cost.

PDB code	Number of iterations with different α										Energy range (kJ/mol)
	0.1	0.2	0.3	0.4	0.5	0.6	0.7	0.8	0.9	1.0	
1ay3 (25)	26	24	22	20	19	18	17	16	15	14	(-271.11, -270.19)
2olx (65)	23	19	16	14	12	11	11	10	9	9	(-559.19, -558.09)
1yjo (121)	31	24	20	17	15	13	12	11	11	10	(-728.89, -727.31)
1etn (180)	33	26	22	19	17	16	14	13	13	12	(-844.68, -842.40)
ala25 (259)	30	23	19	16	14	13	12	11	10	9	(-100.53, -100.32)
1bbl (576)	29	23	19	17	15	14	13	12	11	10	(-3322.1, -3314.6)
PDB code	Number of iterations with different α										Energy range (kJ/mol)
	1.1	1.2	1.3	1.4	1.5	1.6	1.7	1.8	1.9	2.0	
1ay3 (25)	14	13	12	12	11	3	5	7	15	28	(-270.88, -270.04)
2olx (65)	9	8	8	8	7	5	7	9	11	23	(-558.17, -557.67)
1yjo (121)	9	9	8	8	8	3	5	9	11	19	(-728.25, -727.11)
1etn (180)	11	11	10	10	9	9	9	5	7	19	(-842.77, -839.17)
ala25 (259)	9	8	8	7	7	5	3	9	12	22	(-100.42, -100.29)
1bbl (576)	10	9	9	9	8	7	5	7	13	25	(-3315.3, -3313.2)

Table 2: Proteins in water ($\varepsilon_1 = 1$, $\varepsilon_2 = 78.54$, $\kappa = 0.104 \text{ \AA}^{-1}$).

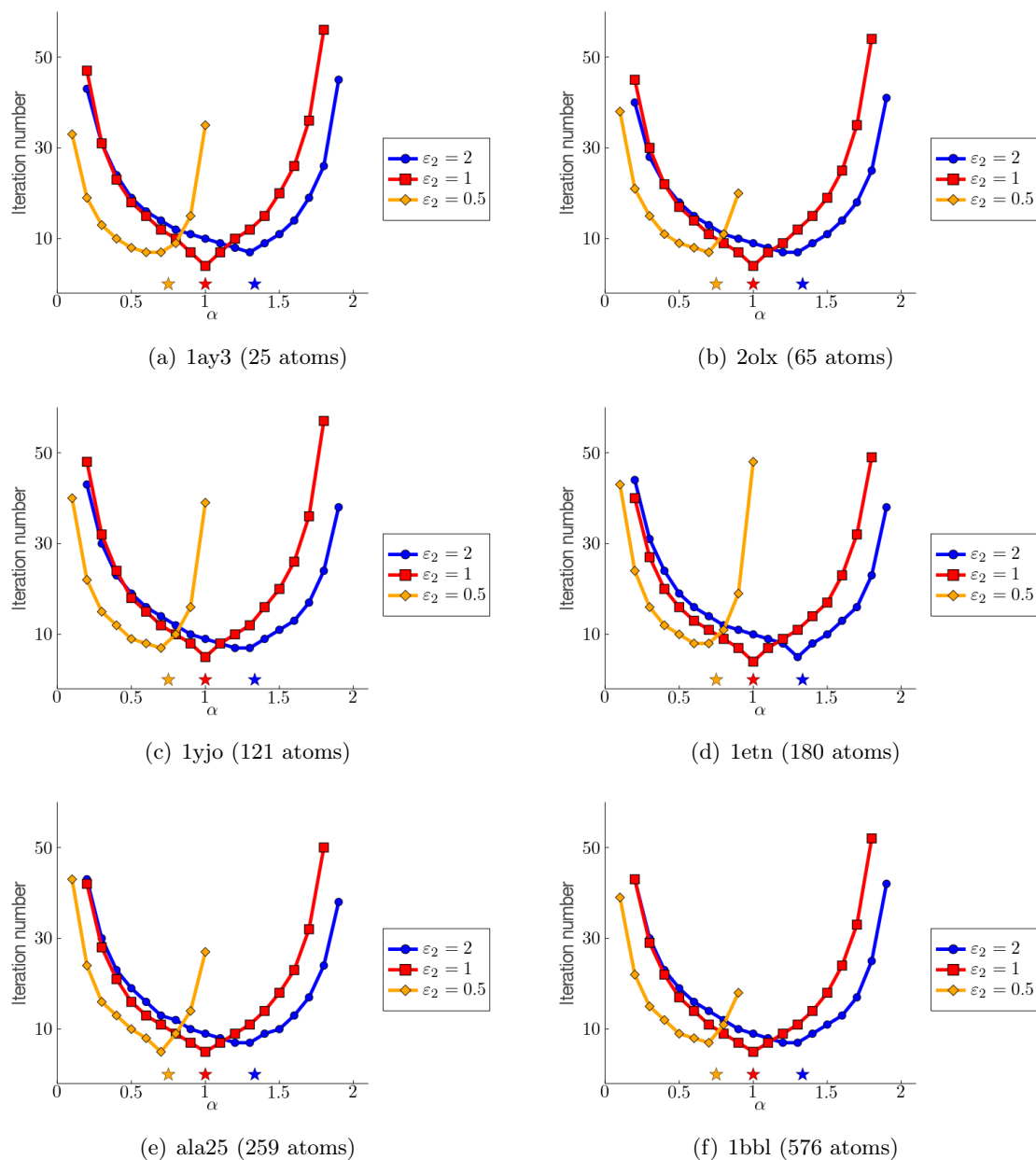


Figure 4: Iteration number $N_{ite}(\alpha)$ vs the stepping parameter α for protein molecules ($\varepsilon_1 = 1$, $\kappa = 0.104\text{\AA}^{-1}$). The optimal parameter α_{op} in (4.7) is the abscissa of star with different colors corresponding different ε_2 .

5 Conclusion

In this work we have proved the convergence of an interior-exterior nonoverlapping domain decomposition method particularly for the linearized Poisson–Boltzmann equation defined in \mathbb{R}^3 . We shall emphasize that our analysis is nontrivial due to the unboundedness of exterior subdomain, that is different from the classical analysis of Schwarz alternating method with nonoverlapping bounded subdomains by Lions. Moreover, a series of numerical simulations have been provided on the optimal choice of stepping parameter for the interior-exterior iteration of the generalized ddLPB method.

Acknowledgement

C. Quan would like to acknowledge Prof. Martin Gander for encouraging to study this topic in a conference at Suzhou. C. Quan and X. Liu would like to thank Prof. Huajie Chen for financial support on our academic communications and discussions.

C. Quan is supported by NSFC Grant 11901281, the Guangdong Basic and Applied Basic Research Foundation (2020A1515010336), the Stable Support Plan Program of Shenzhen Natural Science Fund (Grant No. 20200925160747003), and the Shenzhen Science and Technology Program (Grant No. 20210609104358076).

A Estimation of C_S for a ball

We estimate the newly-defined interior-exterior Sobolev constant C_S for a ball $B_R(\mathbf{0})$. Given some $g \neq 0 \in H^{\frac{1}{2}}(\partial B_R(\mathbf{0}))$, we have

$$u_r(r\mathbf{s}) = \sum_{\ell=0}^{\infty} \sum_{m=-\ell}^{\ell} c_{\ell,m} \left(\frac{r}{R}\right)^{\ell} Y_{\ell}^m(\mathbf{s}) \quad \text{for } 0 \leq r \leq R, \mathbf{s} \in \mathbb{S}^2, \quad (\text{A.1})$$

$$u_c(r\mathbf{s}) = \sum_{\ell=0}^{\infty} \sum_{m=-\ell}^{\ell} c_{\ell,m} \frac{k_{\ell}(r)}{k_{\ell}(R)} Y_{\ell}^m(\mathbf{s}) \quad \text{for } r \geq R, \mathbf{s} \in \mathbb{S}^2, \quad (\text{A.2})$$

where \mathbb{S}^2 is the boundary of the unit ball, $c_{\ell,m}$ is the coefficient of spherical harmonics satisfying

$$g(R\mathbf{s}) = \sum_{\ell=0}^{\infty} \sum_{m=-\ell}^{\ell} c_{\ell,m} Y_{\ell}^m(\mathbf{s}) \quad \text{for } \mathbf{s} \in \mathbb{S}^2, \quad (\text{A.3})$$

and k_{ℓ} is the modified spherical Bessel functions of the second kind [41] with

$$k_{\ell}(r) := \sqrt{\frac{2}{\pi r}} K_{\ell+\frac{1}{2}}(r). \quad (\text{A.4})$$

Here, $K_\alpha(x)$ with the subscript α is the modified Bessel functions of the second kind. Due to the orthogonality of the spherical harmonics, we calculate

$$\|u_r\|_{L^2(\Omega)}^2 = \int_0^R r^2 \sum_{\ell=0}^{\infty} \sum_{m=-\ell}^{\ell} c_{\ell,m}^2 \left(\frac{r}{R}\right)^{2\ell} dr = \sum_{\ell=0}^{\infty} \sum_{m=-\ell}^{\ell} c_{\ell,m}^2 \frac{R^3}{2\ell+3}. \quad (\text{A.5})$$

Multiplying (3.4) with u_c and integrating over Ω^c , we obtain

$$\begin{aligned} \|u_c\|_{H^1(\Omega^c)}^2 &= \langle u_c, \partial_{\mathbf{n}} u_c \rangle \\ &= \int_{\mathbb{S}^2} R \left(\sum_{\ell=0}^{\infty} \sum_{m=-\ell}^{\ell} c_{\ell,m} Y_{\ell}^m(\mathbf{s}) \right) \left(- \sum_{\ell'=0}^{\infty} \sum_{m'=-\ell'}^{\ell'} c_{\ell',m'} \frac{k'_{\ell'}(R)}{k_{\ell'}(R)} Y_{\ell'}^{m'}(\mathbf{s}) \right) d\mathbf{s} \\ &= \sum_{\ell=0}^{\infty} \sum_{m=-\ell}^{\ell} c_{\ell,m}^2 R \frac{-k'_{\ell}(R)}{k_{\ell}(R)}. \end{aligned} \quad (\text{A.6})$$

The modified spherical Bessel functions have the following properties [41] :

$$k_{n-1}(x) - k_{n+1}(x) = -\frac{2n+1}{x} k_n(x), \quad (\text{A.7})$$

$$n k_{n-1}(x) + (n+1) k_{n+1}(x) = -(2n+1) k'_n(x), \quad \text{for } n \in \mathbb{N}, x > 0, \quad (\text{A.8})$$

Since $k_0(x) = \frac{e^{-x}}{x}$, $k_1(x) = e^{-x} \left(\frac{1}{x} - \frac{1}{x^2} \right)$, we know by deduction that $k_n(x) > 0$ and

$$\frac{-k'_n(x)}{k_n(x)} = \frac{k_{n-1}(x)}{k_n(x)} + \frac{n+1}{x} \geq \frac{n+1}{x} \quad \text{for } n \in \mathbb{N}_+, x > 0. \quad (\text{A.9})$$

Then we can estimate

$$\frac{R^2/(2\ell+3)}{(\ell+1)/R} \leq \frac{R^3}{(2\ell+3)(\ell+1)} \leq \frac{R^3}{3} \quad \text{for } \ell \in \mathbb{N}. \quad (\text{A.10})$$

This together with (A.5) and (A.6) leads to

$$\|u_r\|_{L^2(\Omega)} \leq \frac{R^3}{3} \|u_c\|_{H^1(\Omega^c)}, \quad (\text{A.11})$$

implying that

$$C_S = \sup_{g \neq 0 \in H^{\frac{1}{2}}(\partial B_R(\mathbf{0}))} \frac{\|u_r\|_{L^2(\Omega)}}{\|u_c\|_{H^1(\Omega^c)}} \leq \frac{R^3}{3}. \quad (\text{A.12})$$

References

- [1] Byung Jun Yoon and AM Lenhoff. A boundary element method for molecular electrostatics with electrolyte effects. *Journal of Computational Chemistry*, 11(9):1080–1086, 1990.
- [2] Anthony Nicholls and Barry Honig. A rapid finite difference algorithm, utilizing successive over-relaxation to solve the Poisson-Boltzmann equation. *Journal of Computational Chemistry*, 12(4):435–445, 1991.
- [3] Jacopo Tomasi, Benedetta Mennucci, and Roberto Cammi. Quantum mechanical continuum solvation models. *Chemical Reviews*, 105(8):2999–3094, 2005.
- [4] Roberto Cammi and Benedetta Mennucci. *Continuum Solvation Models in Chemical Physics: From Theory to Applications*. John Wiley, 2007.
- [5] Andreas Klamt and GJGJ Schüürmann. COSMO: a new approach to dielectric screening in solvents with explicit expressions for the screening energy and its gradient. *Journal of the Chemical Society, Perkin Transactions 2*, pages 799–805, 1993.
- [6] Michel F Sanner, Arthur J Olson, and Jean-Claude Spehner. Reduced surface: an efficient way to compute molecular surfaces. *Biopolymers*, 38(3):305–320, 1996.
- [7] Yongjie Zhang, Guoliang Xu, and Chandrajit Bajaj. Quality meshing of implicit solvation models of biomolecular structures. *Computer Aided Geometric Design*, 23(6):510–530, 2006.
- [8] Alexander H Boschitsch, Marcia O Fenley, and Huan-Xiang Zhou. Fast boundary element method for the linear Poisson-Boltzmann equation. *Journal of Physical Chemistry B*, 106(10):2741–2754, 2002.
- [9] Michael D Altman, Jaydeep P Bardhan, Jacob K White, and Bruce Tidor. Accurate solution of multi-region continuum biomolecule electrostatic problems using the linearized Poisson-Boltzmann equation with curved boundary elements. *Journal of Computational Chemistry*, 30(1):132–153, 2009.
- [10] Chandrajit Bajaj, Shun-Chuan Chen, and Alexander Rand. An efficient higher-order fast multipole boundary element solution for Poisson-Boltzmann-based molecular electrostatics. *SIAM Journal on Scientific Computing*, 33(2):826–848, 2011.
- [11] Weihua Geng and Robert Krasny. A treecode-accelerated boundary integral Poisson-Boltzmann solver for electrostatics of solvated biomolecules. *Journal of Computational Physics*, 247:62–78, 2013.

- [12] Jiahui Chen and Weihua Geng. On preconditioning the treecode-accelerated boundary integral (TABI) Poisson–Boltzmann solver. *Journal of Computational Physics*, 373:750–762, 2018.
- [13] Jeffry D Madura, James M Briggs, Rebecca C Wade, Malcolm E Davis, Brock A Luty, Andrew Ilin, Jan Antosiewicz, Michael K Gilson, Babak Bagheri, L Ridgway Scott, et al. Electrostatics and diffusion of molecules in solution: simulations with the University of Houston Brownian Dynamics program. *Computer Physics Communications*, 91(1-3):57–95, 1995.
- [14] Lin Li, Chuan Li, Subhra Sarkar, Jie Zhang, Shawn Witham, Zhe Zhang, Lin Wang, Nicholas Smith, Marharyta Petukh, and Emil Alexov. DelPhi: a comprehensive suite for DelPhi software and associated resources. *BMC Biophysics*, 5(1):9, 2012.
- [15] Duan Chen, Zhan Chen, Changjun Chen, Weihua Geng, and Guo-Wei Wei. MIBPB: A software package for electrostatic analysis. *Journal of Computational Chemistry*, 32(4):756–770, 2011.
- [16] Nathan A Baker, David Sept, Simpson Joseph, Michael J Holst, and J Andrew McCammon. Electrostatics of nanosystems: application to microtubules and the ribosome. *Proceedings of the National Academy of Sciences*, 98(18):10037–10041, 2001.
- [17] Todd J Dolinsky, Paul Czodrowski, Hui Li, Jens E Nielsen, Jan H Jensen, Gerhard Klebe, and Nathan A Baker. PDB2PQR: expanding and upgrading automated preparation of biomolecular structures for molecular simulations. *Nucleic Acids Research*, 35(suppl_2):W522–W525, 2007.
- [18] Elizabeth Jurrus, Dave Engel, Keith Star, Kyle Monson, Juan Brandi, Lisa E Felberg, David H Brookes, Leighton Wilson, Jiahui Chen, Karina Liles, et al. Improvements to the APBS biomolecular solvation software suite. *Protein Science*, 27(1):112–128, 2018.
- [19] Long Chen, Michael J Holst, and Jinchao Xu. The finite element approximation of the nonlinear Poisson–Boltzmann equation. *SIAM Journal on Numerical Analysis*, 45(6):2298–2320, 2007.
- [20] Michael Holst, Nathan Baker, and Feng Wang. Adaptive multilevel finite element solution of the Poisson–Boltzmann equation I. Algorithms and examples. *Journal of Computational Chemistry*, 21(15):1319–1342, 2000.
- [21] Nathan Baker, Michael Holst, and Feng Wang. Adaptive multilevel finite element solution of the Poisson–Boltzmann equation II. Refinement at solvent-accessible surfaces in biomolecular systems. *Journal of Computational Chemistry*, 21(15):1343–1352, 2000.
- [22] Eric Cancès, Yvon Maday, and Benjamin Stamm. Domain decomposition for implicit solvation models. *Journal of Chemical Physics*, 139(5):054111, 2013.

- [23] Filippo Lipparini, Benjamin Stamm, Eric Cancès, Yvon Maday, and Benedetta Mennucci. Fast domain decomposition algorithm for continuum solvation models: Energy and first derivatives. *Journal of Chemical Theory and Computation*, 9(8):3637–3648, 2013.
- [24] Filippo Lipparini, Louis Lagardère, Giovanni Scalmani, Benjamin Stamm, Eric Cancès, Yvon Maday, Jean-Philip Piquemal, Michael J Frisch, and Benedetta Mennucci. Quantum calculations in solution for large to very large molecules: A new linear scaling QM/continuum approach. *Journal of Physical Chemistry Letters*, 5(6):953–958, 2014.
- [25] Filippo Lipparini, Giovanni Scalmani, Louis Lagardère, Benjamin Stamm, Eric Cancès, Yvon Maday, Jean-Philip Piquemal, Michael J Frisch, and Benedetta Mennucci. Quantum, classical, and hybrid QM/MM calculations in solution: General implementation of the ddCOSMO linear scaling strategy. *Journal of Chemical Physics*, 141(18):184108, 2014.
- [26] Benjamin Stamm, Eric Cancès, Filippo Lipparini, and Yvon Maday. A new discretization for the polarizable continuum model within the domain decomposition paradigm. *Journal of Chemical Physics*, 144(5):054101, 2016.
- [27] Chaoyu Quan, Benjamin Stamm, and Yvon Maday. A domain decomposition method for the Poisson–Boltzmann solvation models. *SIAM Journal on Scientific Computing*, 41(2):B320–B350, 2019.
- [28] Chaoyu Quan and Benjamin Stamm. Mathematical analysis and calculation of molecular surfaces. *Journal of Computational Physics*, 322:760 – 782, 2016.
- [29] Chaoyu Quan, Benjamin Stamm, and Yvon Maday. A domain decomposition method for the polarizable continuum model based on the solvent excluded surface. *Mathematical Models and Methods in Applied Sciences*, 2018.
- [30] Gabrielle Ciaramella and Martin J Gander. Analysis of the parallel Schwarz method for growing chains of fixed-sized subdomains: Part I. *SIAM Journal on Numerical Analysis*, 55(3):1330–1356, 2017.
- [31] Gabrielle Ciaramella and Martin J Gander. Analysis of the parallel Schwarz method for growing chains of fixed-sized subdomains: Part II. *SIAM Journal on Numerical Analysis*, 56(3):1498–1524, 2018.
- [32] Gabriele Ciaramella and Martin J Gander. Analysis of the parallel Schwarz method for growing chains of fixed-sized subdomains: Part III. *Electronic Transactions on Numerical Analysis*, 49:210–243, 2018.

- [33] Arnold Reusken and Benjamin Stamm. Analysis of the schwarz domain decomposition method for the conductor-like screening continuum model. *SIAM Journal on Numerical Analysis*, 59(2):769–796, 2021.
- [34] Pierre-Louis Lions. On the Schwarz alternating method. I. In *First international symposium on domain decomposition methods for partial differential equations*, volume 1, page 42. Paris, France, 1988.
- [35] Pierre-Louis Lions. On the Schwarz alternating method. III: a variant for nonoverlapping subdomains. In *Third international symposium on domain decomposition methods for partial differential equations*, volume 6, pages 202–223. SIAM Philadelphia, PA, 1990.
- [36] Michael Reed and Barry Simon. *Methods of modern mathematical physics, Volume I: Functional analysis*. Elsevier, 1972.
- [37] Karl E. Gustafson and Duggirala K.M. Rao. *Numerical Range*. Springer, 1997.
- [38] Stefan A Sauter and Christoph Schwab. *Boundary element methods*. Springer, 2011.
- [39] HM Berman, J Westbrook, Z Feng, G Gilliland, TN Bhat, H Weissig, IN Shindyalov, and PE Bourne. The Protein Data Bank. *Nucleic Acids Research*, URL: www.rcsb.org, 28:235–242, 2000.
- [40] Todd J Dolinsky, Jens E Nielsen, J Andrew McCammon, and Nathan A Baker. PDB2PQR: an automated pipeline for the setup of Poisson–Boltzmann electrostatics calculations. *Nucleic Acids Research*, 32(suppl_2):W665–W667, 2004.
- [41] George B Arfken, Hans J Weber, and Frank E Harris. *Mathematical Methods for Physicists: A Comprehensive Guide 7th Edition (London: Academic)*. Academic Press, 2013.